Spatiotemporal Clutter Filtering of Ultrafast Ultrasound Data Highly Increases Doppler and fUltrasound Sensitivity

Charlie Demené*, Thomas Deffieux, Mathieu Pernot, Bruno-Félix Osmanski, Valérie Biran, Jean-Luc Gennisson, Lim-Anna Sieu, Antoine Bergel, Stéphanie Franqui, Jean-Michel Correas, Ivan Cohen, Olivier Baud, and Mickael Tanter

***Abstract*—Ultrafast ultrasonic imaging is a rapidly developing field based on the unfocused transmission of plane or diverging ultrasound waves. This recent approach to ultrasound imaging leads to a large increase in raw ultrasound data available per acquisition. Bigger synchronous ultrasound imaging datasets can be exploited in order to strongly improve the discrimination between tissue and blood motion in the field of Doppler imaging. Here we propose a spatiotemporal singular value decomposition clutter rejection of ultrasonic data acquired at ultrafast frame rate. The singular value decomposition (SVD) takes benefits of the different features of tissue and blood motion in terms of spatiotemporal coherence and strongly outperforms conventional clutter rejection filters based on high pass temporal filtering. Whereas classical clutter filters operate on the temporal dimension only, SVD clutter filtering provides up to a four-dimensional approach (3D in space and 1D in time). We demonstrate the performance of SVD clutter filtering with a flow phantom study that showed an increased performance compared to other classical filters (better contrast to noise ratio with tissue motion between 1 and 10mm/s and axial blood flow as low as 2.6 mm/s). SVD clutter filtering revealed previously undetected blood flows such as microvascular networks or blood flows corrupted by significant tissue or probe motion artifacts. We report *in vivo* applications including small animal fUltrasound brain imaging (blood flow detection limit of 0.5 mm/s) and several clinical imaging cases, such as neonate brain imaging, liver or kidney Doppler imaging.**

***Index Terms*—Blood flow, Doppler imaging, singular value decomposition, ultrafast imaging, ultrasound.**

Manuscript received March 10, 2015; revised April 28, 2015; accepted April 28, 2015. Date of publication April 30, 2015; date of current version October 28, 2015. The research leading to these results has received funding from the European Research Council under the European Union's Seventh Framework Programme (FP7/2007-2013)/ERC grant agreement n° 339244-FUSIMAGINE. This work was also supported by LABEX WIFI (Laboratory of Excellence ANR-10-LABX-24) within the French Program 'Investments for the Future' under reference ANR-10-IDEX-0001-02PSL, by the Assistance Publique-Hôpitaux de Paris and by PremUP Foundation, Paris 75006 France. *Asterisk indicates corresponding author.*

*C. Demené is with the Institut Langevin, CNRS UMR 7587, INSERM U979, ESPCI ParisTech, 75005 Paris, France (e-mail: charlie.demene@espci.fr).

T. Deffieux, M. Pernot, B.-F. Osmanski, J.-L. Gennisson, S. Franqui, and M. Tanter are with the Institut Langevin, CNRS UMR 7587, INSERM U979, ESPCI ParisTech, 75005 Paris, France (e-mail: thomas.deffieux@espci.fr; mathieu.pernot@espci.fr; bruno-felix.osmanski@espci.fr; jl.gennisson@espci.fr; mickael.tanter@espci.fr).

V. Biran and O. Baud are with the INSERM U1141 and Neonatal Intensive Care Unit, Paris Diderot University, Children's hospital Robert Debré, APHP, 75019 Paris, France (e-mail: valerie.biran@rdb.aphp.fr; olivier.baud@rdb.aphp.fr).

L.-A. Sieu is with the Neuroscience Paris Seine, CNRS UMR8246, INSERM U1130, UPMC UMCR18, 75005 Paris, France and also with Institute of Translational Neurosciences (IHU-A-ICM), Pitié-Salpêtrière Hospital, 75013 Paris, France (e-mail: lim-anna_s@hotmail.fr).

A. Bergel and I. Cohen are with the Neuroscience Paris Seine, CNRS UMR8246, INSERM U1130, UPMC UMCR18, 75005 Paris, France (e-mail: antoine.bergel@cri-paris.org; ivan.cohen@upmc.fr).

S. Franqui is with the service de radiopédiatrie-Hôpital Bicêtre-Hôpitaux Universitaires Paris-Sud, Assistance Publique hôpitaux de Paris, 94270 Le Kremlin-Bicêtre, France (e-mail: stephanie.franchi@bct.aphp.fr).

J.-M. Correas is with the Institut Langevin, CNRS UMR 7587, INSERM U979, ESPCI ParisTech, 75005 Paris, France, and also with department of Adult Radiology, Necker University Hospital, 75015 Paris, France, and with Rene Descartes Medical University, 75006 Paris, France (e-mail: jean-michel.correas@nck.aphp.fr).

Color versions of one or more of the figures in this paper are available online at http://ieeexplore.ieee.org.

Digital Object Identifier 10.1109/TMI.2015.2428634

I. Introduction

EXTENSIVE work has been conducted over the past 30 years in order to suppress clutter signals originating from stationary and slowly moving tissue as they introduce major artifacts in ultrasonic blood flow imaging [1]. This operation remains a major challenge for the visualization of vascular paths and the measurement of blood flow velocities because tissue echoes and blood scatterers echoes tend to share common characteristics, especially in two widespread clinical cases e.g., when blood flow velocities become low (in particular in small vessels) or when tissue motion is important. These two configurations correspond both to major applications in general ultrasound imaging. On the one hand, imaging slow blood flows and therefore microvasculature is an issue in most organs as skin, muscles, placenta, as well as in tumors for cancer diagnosis. It is also of major importance in emerging fields such as fUltrasound imaging of brain activity where the neurovascular coupling occurs locally in very small vessels. On the other hand, imaging blood flow in fast moving tissue is a major issue in applications such as cardiac or abdominal (liver, kidney,…) imaging.

The reason why clutter filters fail to solve both situations mentioned above is due to the underlying assumption on which they are built. In the early history of Color Flow Imaging (CFI), clutter filtering has always been based on the fair assumption that tissue signal and blood flow signal have completely differing spectral characteristics: tissue motion is supposed very slow or non-existent whereas red blood cells are fast moving scatterers, meaning that demodulated tissue signal and blood

signal have non-overlapping spectra centered on the zero frequency and the Doppler frequency respectively. Based on this temporal dynamics assumption, the raw ultrasonic signal is filtered along the temporal dimension using finite impulse response (FIR) or infinite impulse response (IIR) filters [2], [3]. IIR filters present the advantage of having steeper roll-off than FIR for a given order, but they also exhibit a longer settling time because of the lack of correct outputs for the first temporal points. FIR filters present a short settling time (output is stable after only n points for an n-order FIR filter) but need a higher order to efficiently discriminate clutter from blood signal. In both cases a first limitation arises: due to real-time requirement and the use of focused ultrasonic beams to build the image, the number of temporal samples available in each spatial location is low (usually 8 to 16) and those filters are really difficult to optimize [4] for a general Doppler imaging application ranging from cardiac imaging (maximal tissue velocity) to microcirculation imaging (very low blood flow speeds). The problem of the settling time can be reduced by a proper initialization [5] in the case of IIR filters but the transient response cannot be completely canceled. On the other hand, another class of filters called standard linear regression (SLR) filters [6] do not exhibit any settling time and estimate the tissue signal by a linear regression on several temporal points of the ultrasound signal: based on the same assumption than mentioned above, it is assumed that the slow variations of the signal are exclusively due to tissue and the rapid fluctuations are exclusively due to blood flow. Finally, several techniques have been developed to adapt to each Doppler imaging situation by compensating background tissue motion: by estimating first tissue velocity and down-mixing the ultrasound temporal signal via a phase correction, the spectrum can be shifted so that the center frequency of the tissue signal match the zero frequency [7], [8]. The signal is then processed using a classical fixed cut-off filter to remove tissue echoes.

In all these methods, only the temporal information has been used because the hypothesis used to discriminate tissue signal and blood scatterers signal focused on their different spectral content. But it can also be noticed that spatial characteristics of tissue signal are different from those of blood scatterers. Along one M-mode line, tissue movement toward the transducer can be approximated by only a shift in the RF data (a phase shift for In Phase/Quadrature RF data) whereas moving red blood cells change the profile of the RF data itself. A brief explanation is that tissue is far less deformable than a red blood cell arrangement in plasma, and a small movement of tissue can be seen as a spatial shift of a speckle pattern whereas a movement of red blood cells implies a reorganization of the scatterers generating a different speckle pattern. In other words, tissue signal has a higher spatial coherence than blood signal in ultrasound imaging. Several authors suggested this hypothesis and introduced new clutter rejection methods based on this a priori: Ledoux *et al.* [9] proposed a clutter reduction simulation study based on the Singular Value Decomposition of the correlation matrix between successive temporal samples of a M-mode line. In this approach both 1D spatial and temporal information are used via the diagonalization of the spatiotemporal (time and depth) correlation matrix. Several strategies have emerged from this approach and an exhaustive review of these methods have been proposed by Yu and Lovstakken in 2010 [10]. Among those developments, important works such as the down-mixing approach using an eigen-based tissue motion estimation of Bjearum *et al.* [8] and the real time implementation of eigen-based clutter rejection proposed by Lovstakken *et al.* [11] have to be cited. Finally, Kruse and Ferrara [12] developed an original high frequency swept scan imaging setup whose datasets have been processed using principal component analysis to estimate blood velocity in presence of strong motion.

In all reported methods, discrimination between tissue and blood flow drastically suffer from a poor ensemble length, i.e., a poor number of ultrasound pulses per line of color. The use of focused beams imposes to adopt a line-per-line scan strategy (either electronically in the case of transducer arrays, or mechanically in the case of a single transducer) in order to cover an extensive field of view. As a consequence both the number of temporal samples (collected on a particular location before the system has to move to another location) and the number of spatial samples (acquired at different times and therefore having different characteristics) are limited. From a theoretical point of view, taking into account different spatial samples along the swept direction is even intrinsically difficult as these samples are not acquired simultaneously. Unfortunately, these characteristics of ultrasonic sequences in conventional ultrasound strongly limit the impact of singular value decomposition. SVD processing is a powerful signal processing tool but as for digital filters its full potential is obtained on large datasets.

Over the past decade, it was shown that ultrafast ultrasound imaging based on unfocused wave transmissions can acquire wide two-dimensional fields of view at very high frame rates (typically higher than 1000 frames per second). The fast growing number of emerging clinical applications of ultrafast imaging [13], [14] and exponential evolution of computation power of GPU based electronics permits to envision a soon change of paradigm in ultrasonic imaging. At the cost of a little loss in focusing capabilities, plane wave imaging enables the acquisition of a large amount of synchronous samples which, in the framework of clutter rejection filters, overcome severe limitations inherent to conventional focused transmissions.

Instead of collecting typically 16 temporal samples in a small spatial box before electronically moving to another location as in conventional Doppler imaging, ultrafast imaging uses plane waves to insonify the medium before beamforming the backscattered echoes into an image. This enables ultrafast imaging over a wide field of view at a framerate of several kHz. As ultrafast imaging relies on focusing in reception only, resolution is partially lost compared to classical ultrasound imaging schemes using focusing both in emission and reception. However, it has been demonstrated that resolution or motion estimation can be improved using a set of tilted plane or diverging waves combined after beamforming [15]–[17]. The ultrasonic modality based on coherent synthetic recombination of unfocused wave transmissions and used to visualize blood flows was called Ultrafast Doppler imaging.

In a former study, we reported that Ultrafast Doppler imaging improved Doppler sensitivity by a factor up to 30 compared

to conventional Doppler imaging [18]. This is in large extent due to the temporal ensemble length of an Ultrafast Doppler dataset compared to a conventional Doppler dataset. As Ultrafast Doppler does not need electronic sweeping of the focused beam along the transducer array, temporal samples are acquired simultaneously in every pixel of the image. This means that for a 1 second acquisition at 1 kHz of frame rate, each pixel exhibits 1000 temporal points. The settling time of temporal filters is not an issue anymore and high order IIR with steep roll-of can be used as long as the first tens of temporal points are removed from the signal. The increased sensitivity of Ultrafast Doppler is in a quite large extent due to this highly efficient clutter filtering combined with a longer ensemble length and a "virtual" [19] dynamic focusing due to coherent recombination of different sonications.

However, to date, the only *a priori* used to filter out the clutter of Ultrafast Doppler Images was based on a temporal discrimination between tissue and blood flow motion [17], [18], [20]. Again, this assumption is not true in the case of slow blood flows or fast moving tissue where both spectra overlap. In these cases, spectral filters applied to Ultrafast Doppler encounter the same difficulties than mentioned previously to discriminate between tissue and blood flow.

In this paper, we present a way of rejecting clutter signals from Ultrafast Doppler datasets using Singular Value Decomposition (SVD) or Principal Component Analysis (PCA). Both 2D spatial and temporal coherence are used to separate tissue from blood flow, showing a considerable improvement in both the detection of slow blood flows and the removal of moving tissues. Thanks to ultrafast sequences, simultaneous raw data can be reshaped under large Casorati matrix form [21]. This article focuses on the straightforward use of singular value decomposition of this Casorati matrix for blood/tissue discrimination. However, the reader should note that very significant developments were achieved in the field of matrix regression in the last five years. Most of them are devoted towards low-rank matrix regression and signal separation, i.e., the so-called Robust PCA [22]. In addition to pure mathematical developments, these techniques have been widely used in other medical imaging modalities like magnetic resonance imaging (MRI) [23] and x-ray computed tomography [24].

II. Theory

A theoretical framework is introduced in this section of the paper to explain the different steps of the clutter rejection algorithm and better understand its implications.

A. The Specificity of Ultrasound Signal

1) The Different Components of the Ultrasound Signal: An Ultrafast Doppler acquisition consists in a stack of beamformed ultrasound images (or a cineloop) and can be represented under the complex valued variable $s(x,z,t)$, where x stands for the lateral dimension (along the transducers array), z stands for depth in the medium in front of the ultrasonic probe, and t stands for time (sampled at a frequency noted Frame Rate from there on). It is assumed that this signal can be described as the summation of three contributions (1): c the clutter signal, b the blood signal, and n the electronical/thermal noise.

$$s(x,z,t) = c(x,z,t) + b(x,z,t) + n(x,z,t). \quad (1)$$

Those three contributions have different spatial and temporal characteristics. n can be considered as a zero-mean Gaussian white noise. The classical approach consists in assuming that blood signal is a high temporal frequency signal and that tissue signal is a low frequency signal. It must be also acknowledged that depending on the ultrasound frequency used for the acquisition, the backscattered energy of the blood signal can be 10 to 60 dB lower than energy of the tissue signal. Moreover, although spatial characteristics of blood and tissue signals are rarely investigated, they also convey different information.

2) Covariance Matrix of Neighboring Pixels: This section elucidates the spatiotemporal characteristics of blood signal and tissue signal, first qualitatively by introducing a simplified signal $\tilde{s}$ to illustrate the common statistical properties of neighboring pixels, and then quantitatively by constructing the covariance matrix of neighboring pixels.

Fig. 1 gives insight into the statistical properties of blood signal b and clutter signal c in the example of rat brain ultrasonic imaging. As stated before the temporal signal in one pixel exhibits low frequency fluctuations corresponding to tissue movement (in the imaginary part of the signal the three slow oscillations observed are due to tissue moving when the heart beats) and high frequency fluctuations due to actual blood cells motion. In order to compare spatially close temporal signals, a simplified signal $\tilde{s}(x,z,t) = s(x,z,t).\overline{s(x,z,t)}^{*}/|\overline{s(x,z,t)}|^2$ is calculated, where $\overline{s}$ is the time average value of s and * stands for complex conjugate. This simplified illustrative representation enables to get rid of any phase shift (via the product with the complex conjugate of the time averaged signal) and of amplitude difference (via the division with the squared modulus) between two pixel signals; and consequently to compare signals only on the basis of their shape. Fig. 1 shows that in neighboring pixels, simplified signals present very similar low frequency variations (tissue motion), whereas the rapid fluctuations (blood motion) do not present the same pattern from one pixel to another. This aspect is further investigated in Fig. 2, where the nine pixel signals of the second neighborhood of Fig. 1 are separated in blood (HF) and tissue (LF) signal with a temporal filter. It is clear that tissue signal is highly correlated and the covariance matrix of those nine signals exhibits a high degree of correlation, whereas the blood signal covariance matrix is almost diagonal, meaning that blood signal is poorly spatially coherent, even at a very local scale. Fig. 1 even shows that at large spatial scales, tissue signal is still quite coherent as the simplified signals are quite similar in shape between the two neighborhoods. Thus, tissue signal could be condensed in a few temporal signal accompanied by a set of spatially arranged complex coefficients required to recover the amplitude and phase shift proper to each pixel. In other words, tissue signal realization in all pixels forms a family of vectors whose cardinality is much higher than the dimension of the tissue vector subspace. This is an essential idea

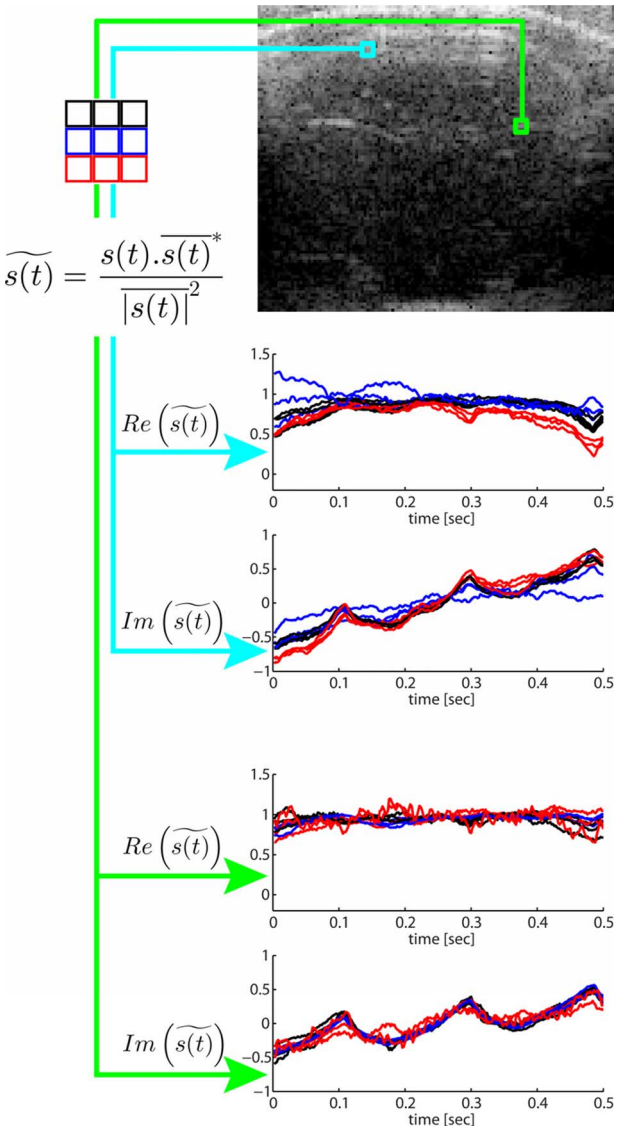

Fig. 1. Typical example of an Ultrafast Acquisition. The top image depicts $s(x, z, t = 0)$ of an Ultrafast acquisition acquired during 0.5 s at a Frame Rate of 500Hz, on the brain of a thinned skull rat (scale bar $= 1$ mm). To have an insight into the temporal dimension of this Ultrafast acquisition, two neighborhoods of nine pixels have been chosen in the image (green and cyan squares). Inside each pixel, the simplified signal $\tilde{s}(x, z, t)$ is calculated to get rid of phase difference and amplitude difference from one pixel to another. $\tilde{s}$ is then plotted with color respective to the position in the nine pixel neighborhood (black, blue or red). This illustrates that signal in close pixels is very similar in shape.

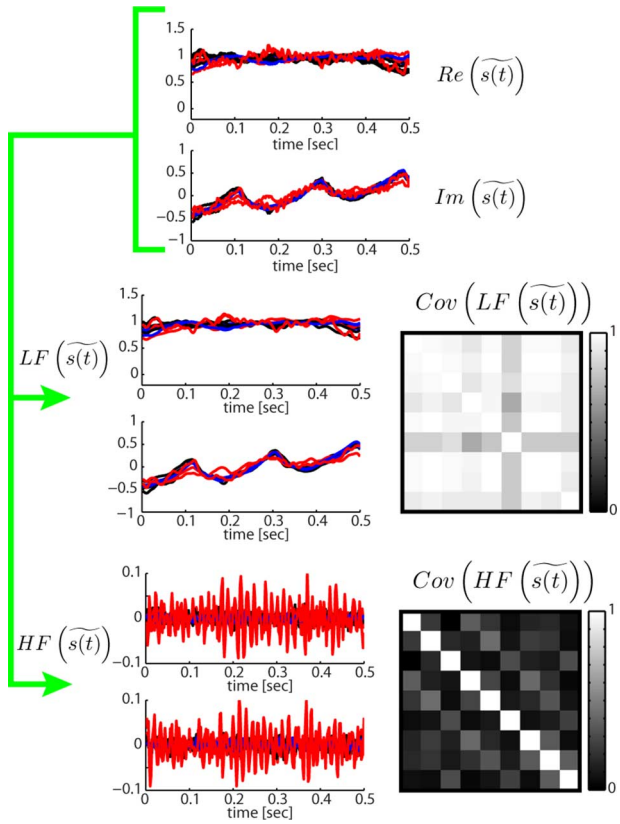

Fig. 2. The same data than in the green nine pixel neighborhood of Fig. 1 are filtered using a 50Hz cut off 4^{th} order Butterworth filter typically used to discriminate between tissue and blood flow signals, and on the graphs it can be observed that the low frequency (LF) part of the nine pixel temporal signal are really similar in shape and seem highly correlated, whereas the blood signal (HF) seem highly decorrelated. On the right are displayed the 9×9 covariance matrix (magnitude) of the normalized zero-mean complex signals, for the low frequency and high frequency part respectively. HF Blood signal is indeed highly decorrelated compared to LF tissue signal.

to understand the efficiency of the singular-based clutter filter presented in this paper.

Contrary to tissue signal, blood signal is not assumed to have high spatial coherence. In addition, tissue signal energy is much higher (10 to 50 dB) than blood signal energy, and a separation method based on covariance estimation certainly finds the highest covariance values for the tissue signal. This discrimination based on covariance estimation can be performed using the singular value decomposition of raw data.

B. Singular Value Decomposition of Ultrafast Ultrasonic Data

Let us consider the spatiotemporal matrix form of $s(x, z, t)$ corresponding to the raw data cineloop acquired during an ultrafast acquisition. $s(x, z, t)$ corresponds to set of $n_x \times n_z \times n_t$ samples where n_x, n_z and n_t are respectively the number of spatial samples along x-direction, the number of spatial samples[1] along z-direction and the number of time samples. The raw data matrix is reshaped under a Casorati matrix form by transforming time series data into a 2D space-time matrix form $\boldsymbol{S}$ with dimensions $(n_x \times n_z, n_t)$ as already proposed in other imaging modalities such as MRI and CT [22]–[26].

The singular value decomposition (SVD) of this Casorati matrix $\boldsymbol{S}$ consists in finding the three matrices such as:

$$\boldsymbol{S} = \boldsymbol{U}\boldsymbol{\Delta}\boldsymbol{V}^*. \tag{2}$$

Where $\boldsymbol{V}$ is a non-square $(n_x \times n_z, n_t)$ diagonal matrix, $\boldsymbol{U}$ and $\boldsymbol{V}$ are orthonormal matrices with respective dimensions $(n_x \times n_z, n_x \times n_z)$ and (n_t, n_t) and * stands for the conjugate transpose. Columns of $\boldsymbol{U}$ and $\boldsymbol{V}$ matrices correspond respectively to the spatial and temporal singular vectors of $\boldsymbol{S}$. One

[1]Note that all concepts described here are straightforwardly applicable for 4D data (3D space +1D time). For sake of simplicity, we restrict here the examples to a 3D case (2D space image + 1D time) which is the most routine case in biomedical ultrasound.

should also notice that $\boldsymbol{U}$ and $\boldsymbol{V}$ also correspond to the eigenvectors[2] of the respective covariance matrices $\boldsymbol{S}\boldsymbol{S}^*$ and $\boldsymbol{S}^*\boldsymbol{S}$.

What is the physical meaning of the SVD of matrix $\boldsymbol{S}$? In fact, the singular value decomposition (SVD) or principal component analysis (PCA) can be thought of as decomposing a matrix $\boldsymbol{S}$ into a weighted, ordered sum of separable matrices $\boldsymbol{A}_i$. By separable, we mean that the matrix $\boldsymbol{S}$ can be written as an outer product of two vectors $A_i = U_i \otimes V_i$. Specifically, the matrix $\boldsymbol{S}$ can be decomposed as:

$$S = \sum_i \lambda_i \boldsymbol{A}_i = \sum_i \lambda_i U_i \otimes V_i. \tag{3}$$

Thus, the SVD can be used to find the decomposition of an ultrafast ultrasonic dataset into separable space and time filters. Here U_i and V_i are the i^{th} columns of the corresponding SVD matrices defined in (6), λ_i are the ordered singular values, and each $\boldsymbol{A}_\text{i}$ is a separable matrix. The number of non-zero λ_i is exactly the rank of the matrix. Importantly, one should keep in mind that each column V_i corresponds to a temporal signal with length n_t and each column U_i corresponds to a spatial signal with length n_t. Each vector U_i describes in fact a 2D spatial image I_i with dimensions (n_x, n_z).

As one can notice, the SVD of $\boldsymbol{S}$ decomposes the field into a sum of separable images I_i (characterized by a vector U_i) that are independently modulated by a temporal signal V_i. In other words, all pixels of the ultrasonic spatial images $I_i(x, z)$ characterized by the singular vector U_i behave with the same time signal $V_i(t)$.

Thus, thanks to the SVD processing, the spatiotemporal cineloop $s(x, z, t)$ corresponding to ultrasonic raw data can be rewritten as:

$$s(x, z, t) = \sum_{i=1}^{rank(\boldsymbol{S})} \lambda_i I_i(x, z) V_i(t). \tag{4}$$

In this decomposition, tissue displacements should be described mainly in the first singular values and singular vectors as their high spatiotemporal coherence insures that a large number of spatial pixels will exhibit the same time profile. On the contrary, blood signal should be found in lower singular values as they exhibit much lower spatiotemporal coherence. Thus, filtering the data using the SVD approach consists in calculating:

$$\boldsymbol{S}^f = \boldsymbol{S}\boldsymbol{V}\boldsymbol{I}^f\boldsymbol{V}^* = \boldsymbol{U}\boldsymbol{\Delta}^f\boldsymbol{V}^*. \tag{5}$$

Where $\boldsymbol{S}^f$ is the filtered data set and $\boldsymbol{I}^f$ is a matrix filter, i.e., the diagonal identity matrix with zeros for the first diagonal elements, leading to a truncated $\boldsymbol{\Delta}^f$ diagonal matrix of singular values corresponding to the removal of tissue motion.

Interestingly, the classical clutter filter approach used in ultrasound imaging corresponding to a simple high pass filter can be written under a quite similar matrix formalism:

$$\boldsymbol{S}^f = \boldsymbol{S}\boldsymbol{E}\boldsymbol{I}^f\boldsymbol{E}^*. \tag{6}$$

[2]Singular Value Decomposition and Principal Component Analysis are two aspects of the same problem and one decomposition can lead to the other and vice versa as $S^*S = V\Delta^*U^*U\Delta V^* = V\Delta^2V^*$ and $SS^* = U\Delta^*V^*V\Delta U^* = U\Delta^2U^*$.

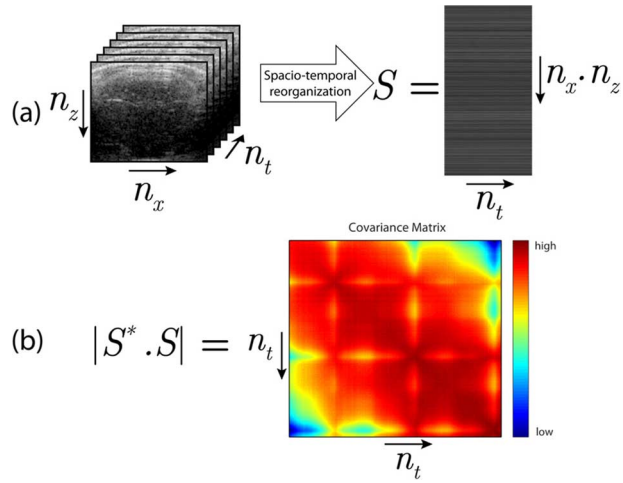

Fig. 3. (a) The ultrafast Doppler acquisition forms a 3D stack of images with 2 spatial dimensions and one temporal dimension (same data than Fig. 1). It is reshaped in one spatiotemporal representation (Casorati matrix) where all pixels at one time point are arranged in one column. As a consequence all time points for one pixel are arranged in one row. (b) The covariance matrix is presented here in magnitude and is of dimension $n_t \times n_t$.

Where $\boldsymbol{E}$ is the Fourier transform matrix and $\boldsymbol{I}^f$ is again the high pass filter, i.e., the diagonal identity matrix with zeros for the diagonal elements corresponding to low frequencies (the first and last ones with a classical FFT algorithm). In the light of this formulation both filters are temporal filters and rank-reducing for the tissue signal (the tissue is compressed on a subset of the spectrum that is then set to zero) but the SVD outperforms the Fourier decomposition according to the Eckart-Young theorem [27] as it provides a faster decrease of singular values and consequently a better tissue blood discrimination. In other words, the decomposition is better in the multidimensional SVD approach as the clutter basis vectors are calculated adaptively (through spatial averaging) and more optimally compared to the Fourier basis.

C. Implementation of the SVD Filter

Given the hypothesis of high spatiotemporal coherence for the tissue signal, the idea is to build a new spatiotemporal representation of the Ultrafast acquisition in the basis provided by the singular value decomposition. The first step is presented in Fig. 3(a) and consists in rearranging the Ultrafast Doppler acquisition into a 2D Casorati matrix $\boldsymbol{S}$ where one dimension is space and the other dimension is time. Singular value decomposition could be performed on this matrix $\boldsymbol{S}$ and directly give the new temporal singular vector basis $\boldsymbol{U}$ and the new spatial singular vector basis $\boldsymbol{V}$.

However, in most cases the Ultrafast Doppler acquisition presents many more spatial points (typically several 10 000) than temporal points (several hundreds or thousands), and it can be less demanding from a computing point of view to first form the $n_t \times n_t$ covariance matrix (Fig. 3(b)) and diagonalize it. This gives n_t temporal eigenvectors that are the right singular vector V_i of $\boldsymbol{S}$. Fig. 4(a) shows the spectral content of those eigenvectors sorted by decreasing eigenvalue. Interestingly, the largest eigenvalues are associated with the temporal singular vectors presenting the slowest variation. This is consistent with

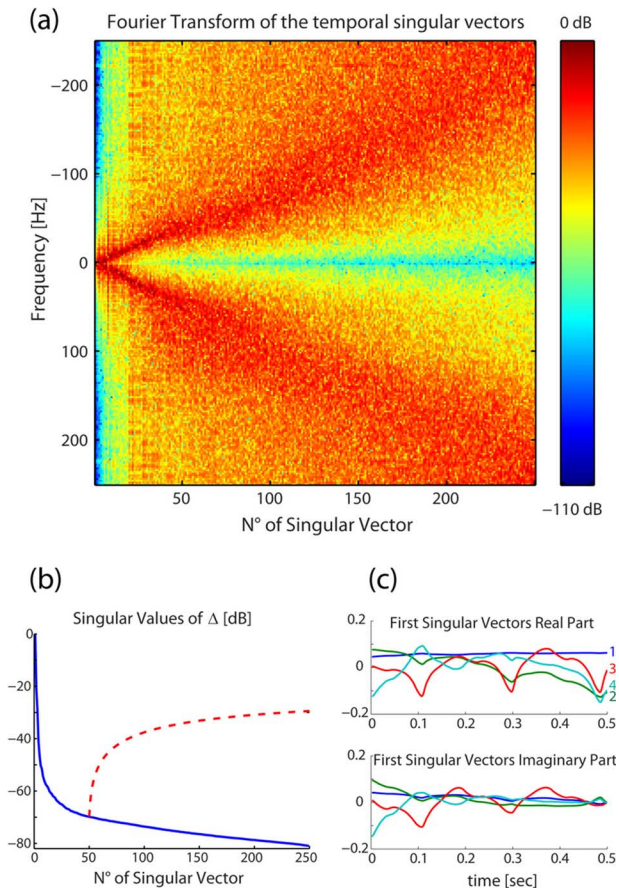

Fig. 4. (a) Spectral content estimation (via Periodogram with Tukey apodisation (0.2)) of all the right singular vectors, sorted with decreasing singular value. Low frequency temporal signal are associated with the highest singular values. As all singular vectors are normalized, energy in all spectra (all columns) is equal to one. (b) Singular values of the matrix Δ (solid blue) expressed in dB and cumulative sum of those singular values from n°50 (dashed red). (c) The first four singular vectors (associated to the largest singular values of the covariance matrix) of the covariance matrix are plotted versus time. It can be observed that they depict slow temporal variation (the first one is almost a constant value, the third one depicts clearly the pulsatility of tissue already observed in Fig. 1) and are devoid of the fast fluctuation of blood signal.

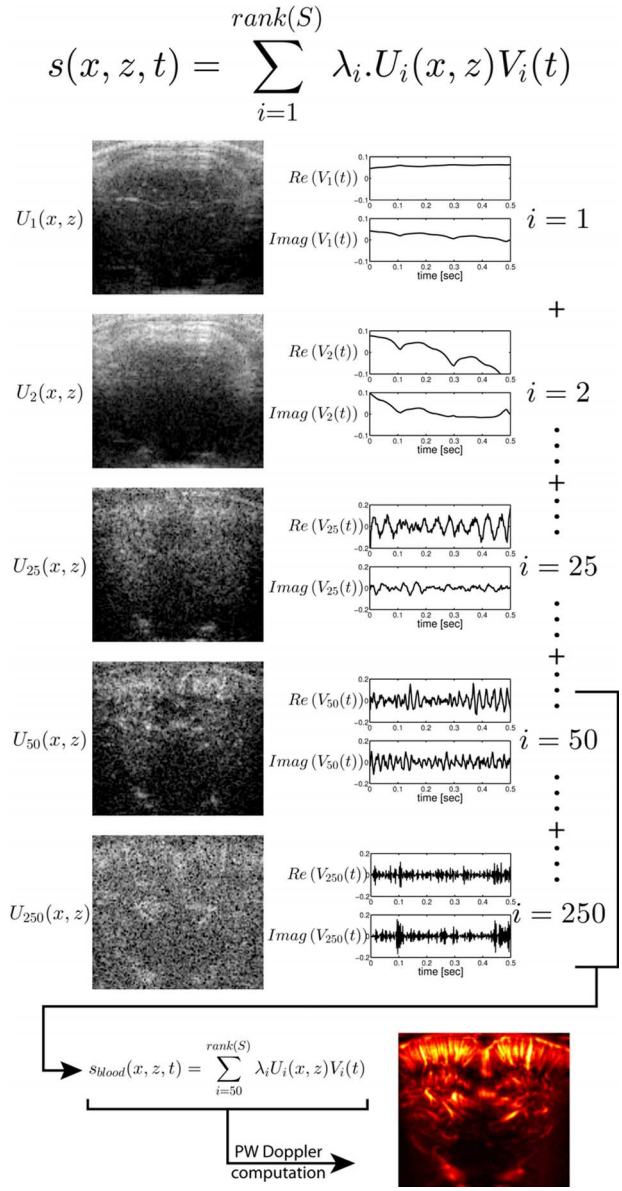

Fig. 5. The Ultrafast acquisition (same data than Fig. 1) is decomposed by the singular value decomposition into a set of spatiotemporal couples of vectors. The essential idea is that tissue signal is coherent enough to be quite similar over the entire image, and that it can be described by a set of vectors constituting a subspace of the temporal signal space, but much smaller. Indeed, by rejecting the first 49 couples of singular vectors, tissue signal is rejected and a very good PW Doppler image of the vascularisation in the rat brain is obtained.

spatially coherent tissue signal supposed to be quite similar in neighboring pixels in a way that enables to reduce the $n_x \times n_z$ realizations of tissue temporal signal on a much smaller subspace. As a consequence tissue signal is supposed to be condensed in the first singular vectors whereas blood and noise signals are described by the singular vectors associated with lower singular values. The eigenvalue itself is closely related to the energy associated the corresponding singular vector and Fig. 4(b) depicts the relative variation of those singular values: the dashed red line shows that with a threshold of 50 rejected singular values (see Fig. 5) the SVD clutter rejection will discriminate the supposedly tissue from a signal 30 dB below, which is really consistent with the expected relative difference between tissue energy and blood energy at that range of US frequencies (15 MHz). The weighted spatial vector $\lambda_i U_i$ are then computed by the projection $\boldsymbol{SV}$ as described in (5).

Finally using this decomposition, $s(x,z,t)$ can be decomposed on both a temporal basis and a spatial basis of singular vectors (Fig. 5). Based on the assumption that tissue signal is gathered in the first singular vectors, clutter rejection is performed using a threshold n (whose influence and choice will be discussed in the next part) on the number of singular vectors removed from the raw signal (7):

$$s_{blood}(x,z,t) = s(x,z,t) - \sum_{i=1}^{n} \lambda_i I_i(x,z) V_i(t). \qquad (7)$$

This filtered signal can then be processed using short time Fourier transform for blood flow speed measurement (as described in the methods section) or the energy per pixel can be computed (8) to produce the so called Power Doppler image.

$$PW(x,z) = \int |s_{blood}(x,z,t)|^2 dt. \qquad (8)$$

The efficiency of clutter rejection based on both space and time filtering of ultrafast data via SVD and its superiority to conventional temporal filtering will be demonstrated in the Results section with a phantom study and with several *in vivo* examples and in different imaging contexts.

III. Materials and Methods

In vivo Ultrafast acquisitions were performed using a programmable ultrasound scanner (Aixplorer, Supersonic Imagine, France) with dedicated Compound Plane Wave imaging ultrasound sequences [17], [16]. This technique uses plane wave emissions instead of the classical focused emissions, which enables to increase the framerate from a factor 10 to 100, and focusing is only achieved in reception via the beamforming process. To recover resolution, compounding is done by coherently adding several tilted plane wave emissions. With such a process, the framerate can reach the theoretical limit imposed by the time of flight of ultrasound, typically 10 000 Hz.

A. Phantom Study

In order to quantify the ability of SVD filtering to extract slow blood flows from moving tissue, a contrast to noise ratio (CNR) study has been conducted with ultrafast Doppler acquisitions on a Doppler phantom in presence of probe movement. The double benefit of using a phantom is to control precisely the acquisition conditions in terms of blood speed and tissue velocities, and to know exactly the geometry and position of the vessel for rigorous calculation of the CNR.

The ultrasonic probe was mounted on a linear motor (PI translation stage VT-80, one-directional repeatability 0.8 μm, bi-directional repeatability ± 10 μm) to enable periodic translation along image depth of amplitude 1 mm with a selected speed (1 to 10 mm/s with 1mm/s incremental steps). The field of view of the probe was adjusted on the longitudinal section of the 2 mm diameter tube of a Doppler phantom (Model 523A, ATS Laboratories, 404 Knowlton St, Bridgeport CT 06608 USA). The tube was approximately at a 35 mm depth, with a 75° angle to the probe axis, giving the possibility of reaching small axial velocities. A blood mimicking fluid (Doppler test fluid model 70, ATS Laboratories, 404 Knowlton St, Bridgeport CT 06608 USA) was injected in that tube with an adjustable pump (Ecoline VC-MS/CA8-6, ISMATEC) enabling mean fluid velocities measured at 1, 2, 4, 6 cm/s (thus 2.6, 5.1, 10.4 and 15.5 mm/s of axial velocities). Ultrafast acquisitions were performed using a 6 angles (ranging from $-5°$ to 5° with 2° incremental steps) compound plane wave ultrasound sequence and a 6 MHz ultrasonic probe (SL 10-2 Supersonic Imagine, France) (pitch 0.2 mm, elevation focus 35 mm, 96% Bandwidth @-6dB). The Pulse Repetition Frequency (PRF) was 6000 Hz, the frame rate of 1000 Hz and the number of frames 600. Twelve acquisitions were performed for each (tissue velocity, blood velocity) couple.

The imaged region of interest was 25.6 mm wide and ranged from 25 mm to 45 mm in depth. The known position of the tube was manually segmented on the BMode (avoiding bias of segmentation on the Doppler image) in order to give two areas (one for the vessel and one for the surrounding phantom (tissue), with a 0.5 mm dead zone in between), and the CNR was calculated as the classical:

$$CNR = \frac{\overline{PW}_{tube} - \overline{PW}_{tissue}}{std(PW_{tissue})}. \tag{9}$$

In this equation $\overline{PW}$ stand for the mean value of the power Doppler signal (in the tube or in the surrounding tissue), and std for the standard deviation. Three filtering methodologies were investigated: the 4^{th} order high-pass Butterworth filter, the varying phase increment down mixing approach described in [8] (consisting in a IQ demodulation using the lag one correlation phase averaged on a 5 pixel column neighborhood) followed by 4^{th} order high-pass Butterworth filter, and the SVD filtering approach. To avoid any bias induced by the choice of the cut off, every cut off has been tested for the three filters (meaning every cut off frequency for the first two methods, and every singular value threshold for the SVD filter), and the one giving the maximum CNR was kept for each (tissue velocity, blood velocity) couple.

B. Rat Brain Imaging

All experiments followed European Union and institutional guidelines for the care and use of laboratory animals. Adult ($>$ 4-week-old) Sprague Dawley rats underwent a surgical thinning of the skull under anesthesia (Ketamine/Xylazine) to enable the propagation of ultrasound. They were then placed in a stereotaxic frame and maintained under 1.5% isoflurane during the time of the acquisition. Ultrafast Acquisition were performed using a 15 angles (ranging from -14° to 14° with 2° incremental steps) compound plane wave ultrasound sequence and a 15 MHz ultrasonic probe (Vermont, France) (pitch 0.08 mm, elevation focus 8 mm). Pulse Repetition Frequency (PRF) was 7500 Hz, enabling a frame rate of 500 Hz, enough to correctly sample axial blood flow speeds up to 2.6 cm/s. Ultrafast Doppler acquisitions lasted 0.5 s, enough to acquire 250 frames and to capture 3 cardiac cycles). Data are used for Fig. 1 to Fig. 5 and for Fig. 7.

C. Neonates Brain Imaging

Ultrafast Acquisition were performed using a 6 angles (ranging from $-5°$ to 5° with 2° incremental steps) compound plane wave ultrasound sequence and a 6 MHz ultrasonic probe (SL 10-2 Supersonic Imagine, France) (pitch 0.2 mm, elevation focus 35 mm, 96% Bandwidth @-6dB). Pulse Repetition Frequency (PRF) was 6000 Hz, enabling a frame rate of 1000 Hz, enough to correctly sample axial blood flow speeds up to 10.3 cm/s. Ultrafast Doppler acquisitions lasted 1 s, enough to acquire 1000 frames and to capture 2 to 3 cardiac cycles). This observational study was approved by the institutional review board (CCP: 'Comité de Protection des Personnes', i.e., Committee for the Protection of Persons, CCP agreement N°120601) and local ethical committee, and strictly complies with the ethical principles for medical research involving human subjects of the World Medical Association Declaration of Helsinki, and written consent was obtained from parents of participants. Data were obtained via a transfontanellar (anterior fontanel) Ultrafast Doppler acquisition of a brain parasagittal

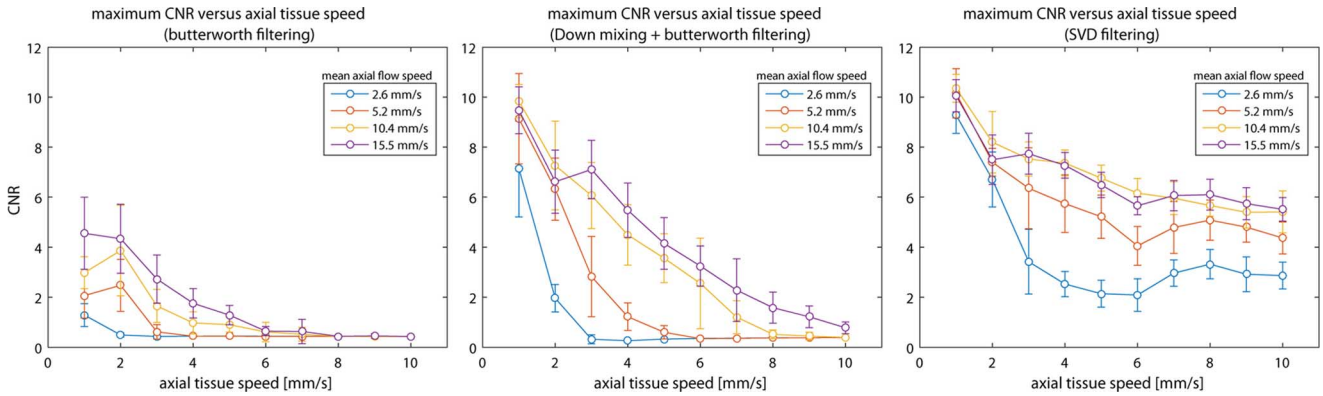

Fig. 6. Evolution of the CNR versus axial tissue velocity for various blood flow speed: phantom study. The same sets of data have been processed using 4^{th} order butterworth high pass filtering (left), down-mixxing prior to 4^{th} order butterworth high pass filtering (middle), and SVD filtering (right). For each measurement, the maximum CNR was found by testing all the possible cut off, and for each experimental condition twelve measurements were pooled to compute mean value (graph circles) and standard deviation (error bars).

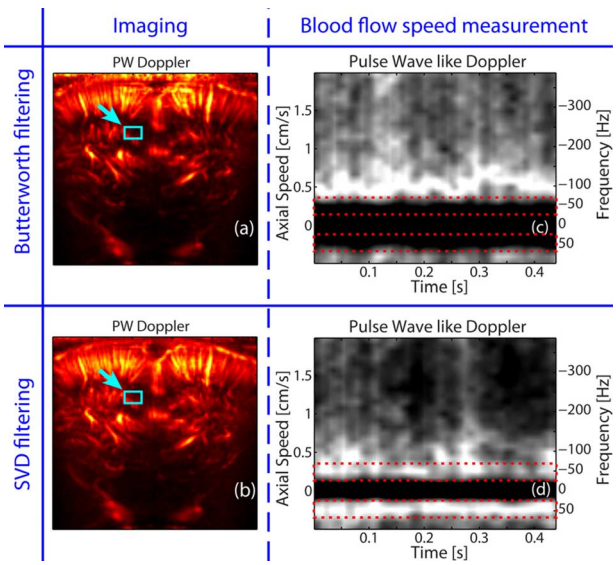

Fig. 7. Comparison of slow blood flow detection (critical for functional imaging) via temporal filtering and SVD filtering (same data than Fig. 1). In that case the rat is maintained in a stereotaxic frame and the probe is maintained in a probe support, the entire setup lying on an anti-vibration table. As a consequence the motion is minimum and consists only in the tissue pulsatility due to blood pressure changes during the cardiac cycle. The PW Doppler image obtained via temporal filtering (50Hz cut off frequency 4^{th} order Butterworth filter) (a) can be compared to the PW Doppler imaged obtained via SVD (b). The cyan arrow indicates the set of pixels where a pulse wave like Doppler profile has been calculated from the Ultrafast Doppler acquisition, in the case of Butterworth filtering (c) and SVD filtering (d). The key point here is the difference between the spectral bands cut by both filters. Blood signal energy is kept via SVD filtering in the two area surrounded by the dotted red rectangles.

section performed *in vivo* on a human neonate and Data are used for Fig. 8 to Fig. 11.

D. Kidney Imaging/ Liver Imaging

Probe and acquisition parameters were the same as for neonate imaging, except (angles: -3°3°; frame rate: 3000 Hz) for liver imaging, and (angles: -5° to 3°, step 2°; frame rate 1600 Hz) for kidney imaging.

Concerning pediatric liver imaging, the observational study was approved by the institutional review board (CCP: 'Comité de Protection des Personnes', i.e., Committee for the Protection of Persons, CCP agreement N° PP-14020) and local ethical committee, and strictly complied with the ethical principles for medical research involving human subjects of the World Medical Association Declaration of Helsinki, and written consent was obtained from parents of the participants. Data are used for Figs. 12 and 13.

Kidney transplant imaging was incorporated in the framework of a study conducted to assess whether Ultrafast Doppler could help providing a parametric map of the transplant vascularization and assessing normal and abnormal vascularization within the transplant to detect fibrosis and inflammation. This clinical study was approved by the French national authorities (clinical trial number 2012-A01070-43). After imaging the morphology of the kidney with Bmode, imaging of the renal transplant vascularization was performed by one radiologist (J.M.C) in the longitudinal axis with conventional Doppler Imaging. Once a good imaging plane was found the Ultrafast Doppler acquisition was launched. Data are used for Figs. 13 and 14.

E. Signal and Image Processing

Each Ultrafast Doppler acquisition was filtered using either a 4^{th} order butterworth filter with a 'symmetric' initialization (mirror reflecting of the 20 first points of the signal) and those first 20 points where then removed to cancel any settling time of the filter, or using the SVD filter described in this paper, or using the varying phase increment down mixing approach described in [8] (Figs. 6 and 11) prior to the same 4^{th} order Butterworth filtering. The PW Doppler image was then calculated as the square root of the mean value of the squared filtered signal (thus corresponding to the energy normalized by the number of samples). This raw data was used directly for the CNR computations of the phantom study. In order to improve visualization for the reader and for fair comparison without inducing perceptive bias, for the all clinical examples PW Doppler images (regardless of the filtering process) were normalized with the highest value at 1 and the minimum value at 0, and histogram equalization was performed with rigorously the same parameters to improve the reader visualization without inducing any perceptive bias.

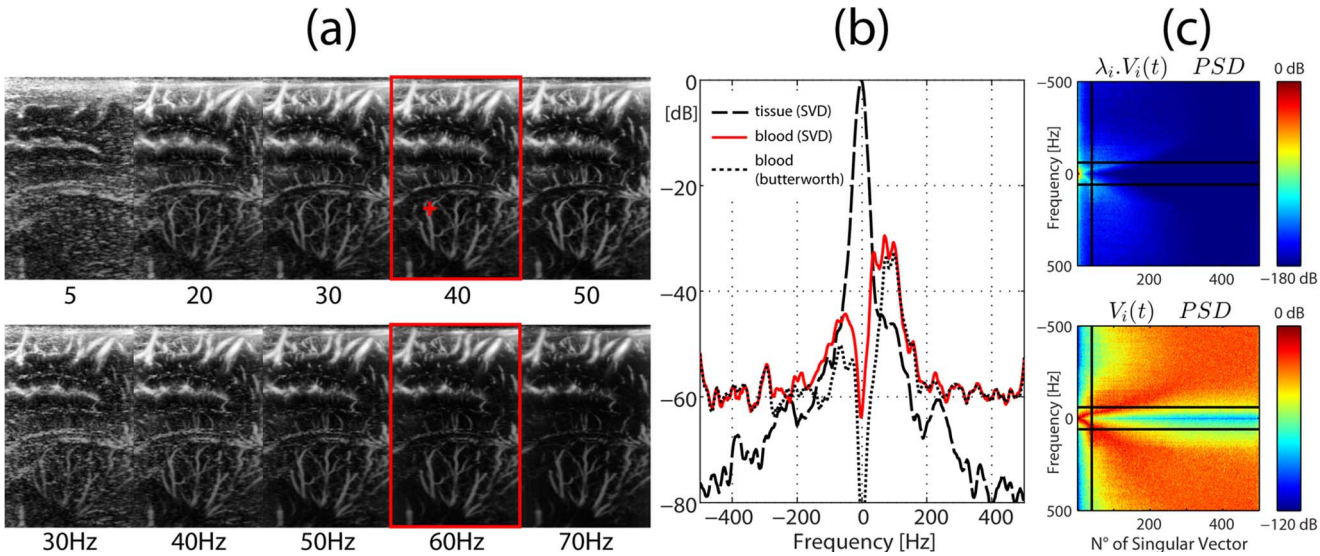

Fig. 8. Comparison between temporal filtering and SVD filtering, the ideal case: no motion and significant blood flow. (a) Effect of both increasing the number of rejected singular values (top) and increasing the temporal filter cut off frequency (bottom) on an Ultrafast Doppler acquisition (brain neonate imaging). For both methods the image that gave the best clutter rejection according to the clinicians has been framed in red. A region of interest has been chosen (red cross) in a vessel and power spectral estimation has been computed on the tissue signal (black dashed line) and blood signal (red solid line) *extracted via SVD filtering*, and blood signal (black dotted line) extracted via temporal Butterworth filtering (b). (c) Spectral diagrams (see Fig. 4(a)) (PSD stands for Power spectral Density): on top weighted with the singular value and on the bottom without weighting. Black lines represent temporal (horizontal) and singular-based (vertical) filtering of the signal.

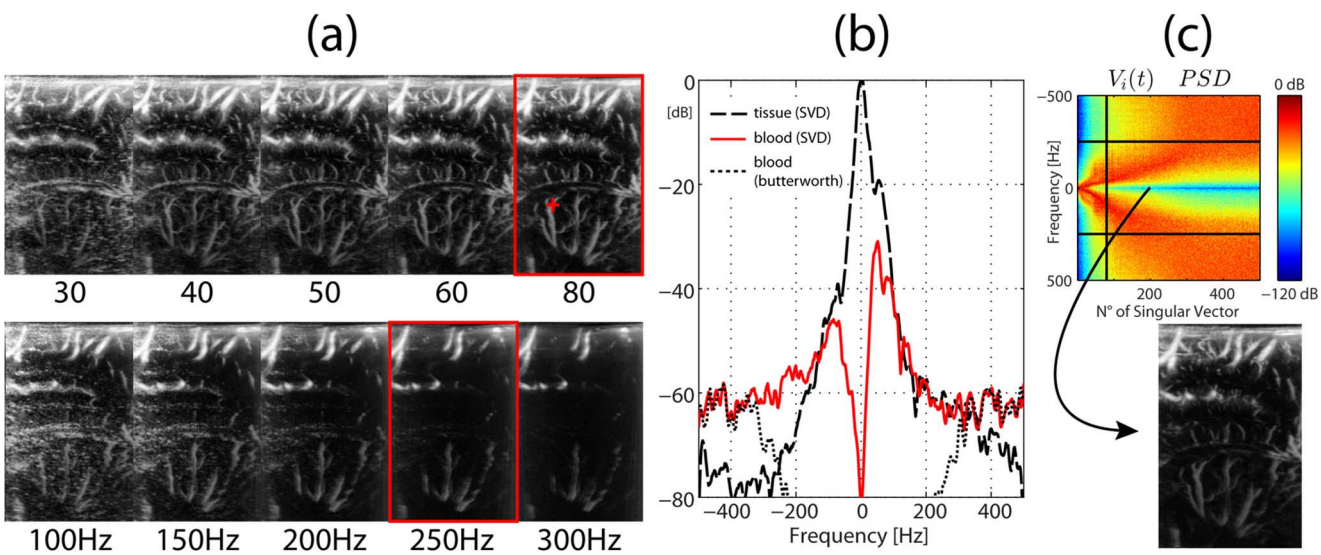

Fig. 9. Comparison between temporal filtering and SVD filtering, the strong motion case. Explanation of the different elements is the same than in Fig. 8, except for the image in (c) which depicts the image build from the energy lost in temporal filtering but kept in SVD filtering (i.e., the content of the energy in the rectangle drawn on spectral diagram top (c)).This acquisition was done 2 seconds after Fig. 8, the only difference is that strong motion was present in the moment of the acquisition.

The spectrograms of Figs. 7(c), 7(d) were generated via short time Fourier transform (32 samples sliding window, lag 2) on the temporal dimension of the pixels in the ROI. Each Fourier transform (meaning each column of the spectrogram) has its maximum set to 1 in order to improve readability. The spectrograms were then averaged in magnitude to be representative of the spectral content (linked to the axial velocity) in the ROI.

IV. Results

A. Phantom Study

The phantom study enabled to quantify the improvement of Ultrafast Doppler detection ability by using SVD filtering versus other well-known methods (high-pass filtering, without or with down mixing) in various experimental conditions representative of the clinical setting for the detection of small vessels: low (1 mm/s) to important (10 mm/s) tissue motion and moderate (15.5 mm/s) to slow (2.6 mm/s) blood flow. Results of this study are presented in Fig. 6. It is striking to notice that even for very small tissue motion, the Butterworth filter alone gives very low values of CNR due to remaining clutter signal, compared to the two other approaches. If a reference value of 2 for the CNR is chosen for discrimination between tissue and flow, the Butterworth filter is unable to extract any blood signal of the explored blood speeds range as soon as

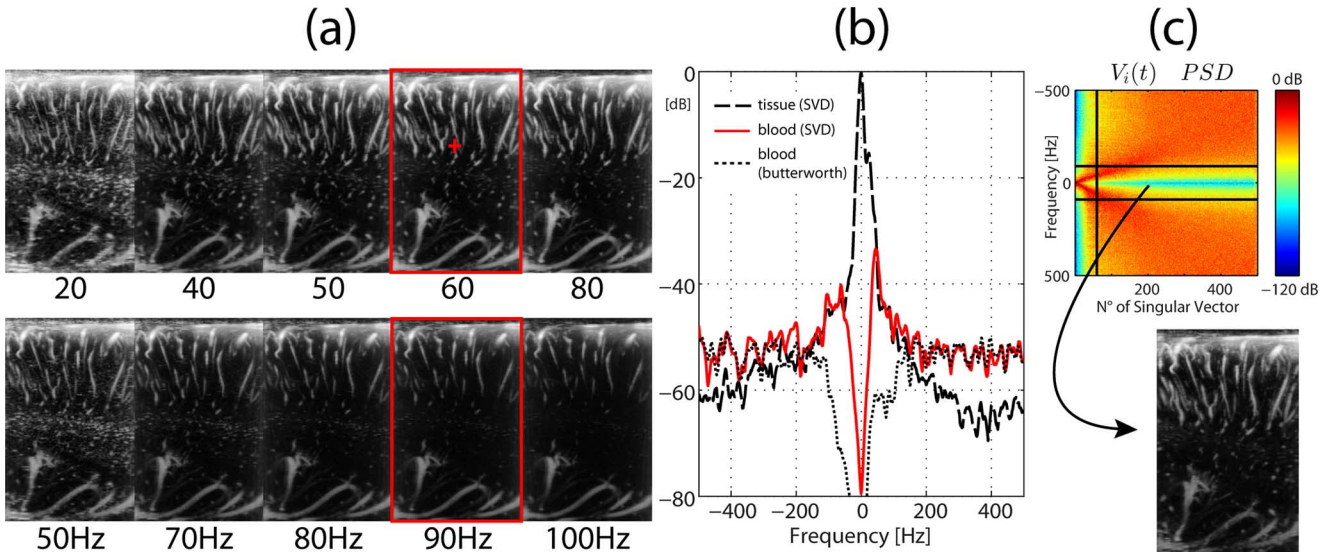

Fig. 10. Comparison between temporal filtering and SVD filtering, the very slow blood flow case. Explanation of the different elements is the same than in Fig. 9. This acquisition has been done in a parasagittal plane where blood vessels are smaller than in Figs. 8 and 9. The interest here is to show that without motion but in case of extremely slow blood flow, SVD filtering can still extract signal that could not be extracted via spectral discrimination.

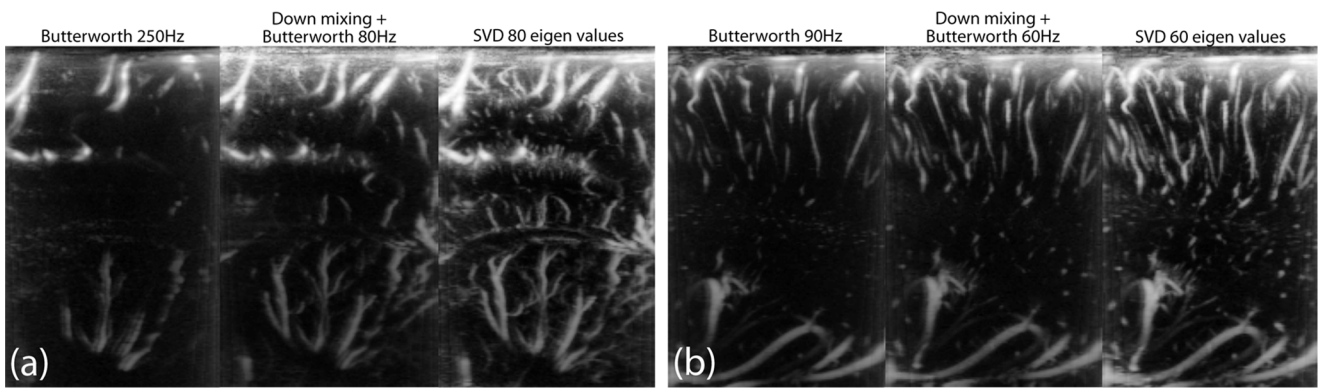

Fig. 11. Comparison of Butterworth filtering, down-mixing prior to Butterworth filtering and SVD filtering . (a) and (b) The data are the same than in Figs. 9 and 10 respectively and in each case the three images obtained with the best possible clutter rejection according to the clinician are presented side by side and in a larger format to enable proper comparison. Higher contrast and better small vessels delineation in the case of SVD filtering are unquestionable.

tissue motion exceeds 4mm/s. The lowest value of blood flow speed (2.6 mm/s) is not detected even for very low tissue speed (1 mm/s). This is not surprising as a spectral method cannot separate 2 signals with comparable speeds and an unfavorable 40 to 60 dB difference of energy. For very slow tissue velocity (1 mm/s) the down mixing approach and the SVD filtering give comparable results, except maybe at the slowest blood velocity that is better extracted via SVD filtering. But as soon as the tissue motion increases (tissue motion $>$ 4 mm/s), the CNR of the down mixing approach decreases rapidly whereas the SVD filtering seems more robust and tends to reach a plateau. This is due to fact that even if down mixing enables to bring back the spectrum of the tissue around the 0 Hz frequency, if the spectral content of tissue and blood flow are too overlapping because of comparable velocities they cannot be efficiently separated by a Fourier based filter, whereas the SVD filter can. SVD filtering appeared to be very robust in this configuration, since we measured a CNR above 2 for all the tested configurations, even when the mean axial blood flow velocity was lower than the tissue velocity (for a blood flow of 5.2 mm/s and a tissue motion of 10 mm/s, the CNR was 4.4$\pm$0.6; for a blood flow of 2.6 mm/s and a tissue motion of 10 mm/s, the CNR was 2.9$\pm$0.5).

B. The Functional Imaging Case

A first comparison of SVD clutter filtering and IIR Butterworth filtering is given (Fig. 7) in the framework of functional ultrasound imaging of brain activity (fUltrasound) [18], [20], [27], [28]. In fUltrasound, it is required to achieve high sensitivity Doppler imaging in order to track the hemodynamic changes due to neurovascular coupling occurring in very small vessels (i.e., mm/s blood flows). This figure is of capital importance to understand how SVD filtering improves both imaging and quantification enabled by Ultrafast Doppler. Figs. 7(a) and 7(b) show the comparison between the Power Doppler (PW) images obtained using SVD and temporal high pass filtering respectively on a thinned skull rat brain. The threshold for singular values and cut-off frequencies were chosen in order to provide the best image quality for both approaches respectively. The key point of this figure lies in the difference of detection of low flow speed depending on the filter.

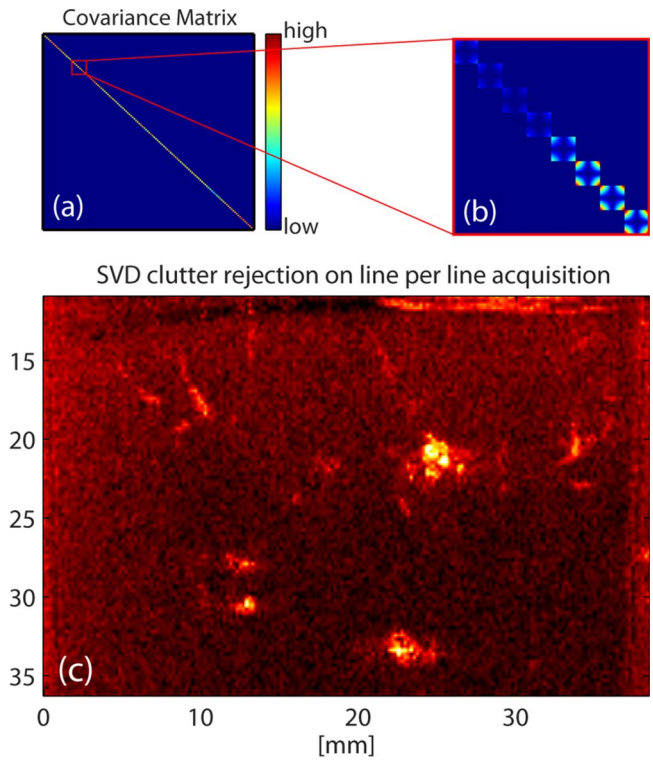

Fig. 12. Importance of the ensemble length for SVD Doppler filtering. An Ultrafast Doppler acquisition has been processed as if it were a line per line acquisition typical of focused ultrasound processed with the method described by Ledoux [9]. Instead of using all the data in the 3D matrix, only are kept the temporal points 1 to 16 for the first column of pixels, the temporal points 17 to 32 for the second column of pixels, and so on. This simulates a swept scan Doppler imaging strategy and the consequence is a lower ensemble length both for space and time. (a) Compared to the covariance matrix of Fig. 3, the covariance matrix for line per line acquisition is very sparse, with only 16×16 blocks on its diagonal. (b) a zoom on a small subregion on the covariance matrix reveals the small 16×16 blocks. (c) The Power Doppler image has been obtained using a SVD filter on each block of the covariance matrix, as would have been done in [9], with a removal of only the first singular vector. The image exhibits very poor sensitivity, and has to be compared to Fig. 13(a) which show the SVD filter result on the full matrix.

Pulse Wave Doppler is the classical ultrasound modality used to monitor the evolution of blood flow speed in one location of the image. The particularity of Ultrafast Doppler acquisition is that this kind of blood flow speed profile can be *a posteriori* computed in every location of the image, as described in [30]. A "Pulse Wave like" Doppler spectrogram can be computed in every pixel of the Ultrafast Doppler acquisition via short time Fourier transform of the In Phase/Quadrature signal, and has been calculated and averaged in magnitude over the region of interest (the set of pixel depicted by the cyan arrow) in both filtering cases (Figs. 7(c), 7(d)). What is of first importance on those spectrograms is the difference between the two filtered out bands of frequency depicted by the dashed red rectangles: the SVD filter is able to reject clutter without cutting entirely a the spectral band where tissue and flow are mixed, giving access to blood flow speed as low as 0.5 mm/s, whereas the 50 Hz cut off butterworth filter tends to cut everything below 2.5 mm/s. This explains why the smallest vessels are better detected via SVD filtering than via butterworth filtering, and in the case of fUltrasound, this difference is primordial since neurovascular coupling occurs at the capillary level, and the blood flow speed in the latter is known to be included in the 0.5-1.5 mm/s range [31].

C. Clinical Imaging

1) The Ideal Doppler Case: Beyond small animal imaging, the next comparisons are performed in clinical settings. A qualitative comparison of SVD clutter filtering and IIR Butterworth filtering is given by Fig. 8 to Fig. 10. The first example (Fig. 8) depicts the vasculature of cortical and thalamic areas. Motion is quite low during this acquisition and blood flow speeds are moderate (2 cm/s to 8 cm/s). Several values have been chosen for the number of rejected singular values and the cut off frequency of the butterworth filter and resulting Power Doppler images are presented. Out of the five examples presented, the best clutter rejection is obtained for 40 rejected singular values and 60 Hz of cut off frequency for SVD processing and conventional temporal filtering respectively. Even though this imaging situation is ideal (no motion artifacts) for the Butterworth high pass filtering, the number of visible blood vessels is bigger for SVD filtering than for Butterworth high pass filtering. It can be noticed that contrast is slightly higher with SVD filtering than with temporal filtering. Contrary to previous publications [4]–[6], [8]–[10] that only give a schematic or simulated representation of spectral distribution for tissue and blood signal, the large ensemble length available with Ultrafast Doppler enables to truly plot the spectral content of blood and tissue signal extracted via SVD filtering and to explain why in general SVD presents a better clutter rejection than temporal filtering. This has been done for each case (Fig. 8(b) to Fig. 10) where the spectral content of tissue signal (black dashed line) and of blood signal (red solid line) of the ROI defined on the image by a red cross mark and extracted via SVD are displayed. As a comparison the blood signal filtered via Butterworth filtering has also been plotted (black dotted line). In this imaging situation noise signal is roughly 60 dB below tissue signal, so the tails of the red solid spectra are mostly noise and not blood signal. In Fig. 8 it is clear that blood and tissue can be separated via temporal filtering because energy of blood signal is higher than energy of tissue in a certain spectral band (50 to 150 Hz), which is a required condition for the vessel to be detected in Power Doppler. This is the reason why temporal filtering gives quite good results in this first example. However it can be observed that the energy of blood signal extracted in the SVD processing is higher than in the temporal filtered extracted blood signal, which illustrates why SVD clutter rejection gives generally better contrast than temporal filters.

Fig. 8(c) represents the spectral content of $\lambda_i V_i(t)$ (upper image) and of $V_i(t)$ (lower image) versus the rank i of the singular value λ_i. On this representation in the singular vector space, the superimposed horizontal black lines represent the cutoff threshold of best Butterworth filtering and the vertical black line represent the cut-off threshold of best SVD filtering (vertical black line). The first image (top) enables to comprehend the relative differences in energy from the first singular vector to the last one, whereas the second one (bottom) enables to observe the differences between normalized spectral contents of individual temporal singular vector. For blood/tissue

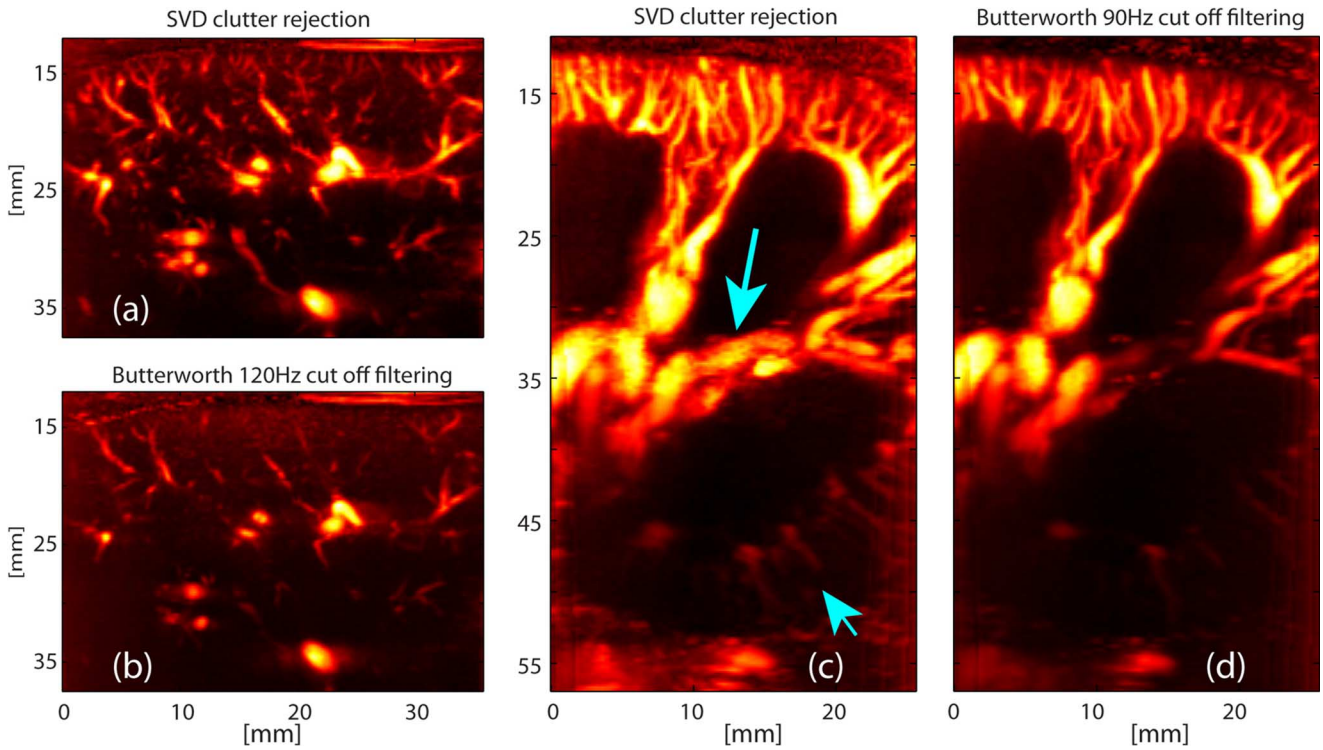

Fig. 13. Clinical examples of filtering improvement via SVD clutter rejection: (a) Ultrafast Doppler acquisition on a child (8 years old) liver processed via SVD, much more small vessels are detected than with butterworth filtering (b). (c) On a transplanted kidney, Ultrafast Doppler gives very good sensitivity with both processing but the few vessels with low flow speed (large vein, long arrow) (very small arteries, deep in the organ, small arrow) are almost completely filtered out by butterworth filtering (d).

discrimination, the first image may be the most important, because it represents the repartition of the total signal energy in a frequency-singular value space: trying to maximize the energy of blood signal over tissue signal in a Power Doppler image is related to the maximization of the integration of the energy in a portion of this frequency-singular value space. In the case of temporal filtering this subspace is chosen as the two rectangles above and below the two horizontal black lines, whereas in the case of SVD clutter rejection this subspace is chosen as the rectangle on the right of the vertical black line. With this representation the double advantage of SVD filtering over temporal filtering is obvious: whereas the latter leaves the "tails" of the tissue spectrum in the filtered signal and removes a great part of blood signal energy (low speeds), the vertical boundary of SVD filtering is much more optimal for the separation of tissue and blood. This explains the higher contrast for the SVD filtered Power Doppler image: although the main part of tissue signal is filtered by temporal Butterworth filtering, the huge difference of amplitude between tissue echoes and blood echoes makes the integration of the energy of tissue signal in the remaining spectral band not negligible compared to the integration of blood signal energy. Also a small part of blood signal is removed between the two horizontal lines.

2) The Strong Motion Case: In the presence of motion this difference becomes tremendous. Fig. 9 presents an acquisition done only two seconds after Fig. 8, but the neonate moved a little bit during this second acquisition, resulting in a strong motion artefact on the Power Doppler image. To recover a complete clutter rejection the cut off frequency of the temporal filtering as to be set to as high as 250 Hz (sampling frequency 1000 Hz) whereas a slight increase to 80 rejected singular values is enough in the case of SVD filtering. Even if a certain level of clutter is tolerated, any image processed with temporal filtering is far from depicting as much vessels as the SVD filtered image. The effect on the Power Doppler is obviously explained by the frequency-singular value diagram presented in (c): to filter pronounced high frequencies in the tissue signal, the temporal filter strategy is to increase the gap between the two horizontal lines, and almost completely filters out the blood signal. As depicted in the central spectrum (b), the vessel marked by the red cross mark would never be detected by temporal filtering because its energy is below tissue signal in every spectral domain. In Fig. 9(c) is displayed the Power Doppler image computed from the energy lying in the rectangle delimited by the singular-value threshold and the two cut off of the temporal filter. In other words it is the blood energy lost by the temporal filter compared to the SVD filter. It shows that a large amount of information is lost in the small vessels when using a temporal filter instead of the SVD filter.

3) The Very Slow Blood Flow Case: The last example in Fig. 10 shows that even with no motion artifacts, SVD filtering is much superior to detect really small vessels whose blood speed is not high enough to get out of the tail of the spectral content of tissue signal (red cross mark: a vessel appearing in SVD processed Power Doppler image and not in temporally processed Power Doppler image). Once again the contrast is higher with SVD processing. Finally, a zoomed view of the optimized Power Doppler images obtained respectively for temporal filtering, down mixing prior to temporal filtering, and SVD filtering is presented in Fig. 11 in order to emphasize the ability of multidimensional SVD filtering to provide better contrast and detect smaller vessels.

D. The Importance of the Plane Wave Imaging Ensemble Length

It was emphasized in the introduction that SVD filtering takes advantage of the large ensemble length provided by the Ultrafast Doppler technique compared to the classical focused emission technique. This is of primordial importance and is illustrated in Fig. 12. In this figure, Ultrafast Doppler data are processed as if they had been acquired with a swept scan strategy used in conventional Doppler: only the temporal points 1 to 16 are kept for the first column of the image, then only the temporal points 17 to 32 are kept for the second column and so on. This simulates a swept scan strategy used in CFI where only 16 temporal samples can be acquired per line because of the need to electronically quickly move to another location. Those data are then processed as proposed by Ledoux in [9]. The huge difference with Ultrafast Doppler SVD filtering lies both in the small number of temporal point acquired in each location and the lack of simultaneity of these temporal acquisitions, and that difference can be understood directly by looking at the covariance matrix: in each block of the covariance matrix the SVD filter has to find a subspace for tissue. As a consequence its ability to efficiently compress the tissue signal on a few singular vector before the subtraction operation is highly impaired.

V. Discussion

SVD clutter rejection has been shown to improve significantly the sensitivity of Ultrafast Doppler in various imaging situations. It is especially efficient in two situations of major interest in Doppler imaging. It removes strong motion artifacts occurring during freehand exams usually downgrading the Doppler image quality. It also strongly improves detection of small vessels characterized by low flow speeds even if mild motion is present. For all studied configurations, SVD clutter rejection provided at least a higher contrast and generally superior detection capabilities. The outperformance of SVD clutter rejection is intrinsically linked with the ultrafast data acquisition. By providing multidimensional simultaneous ultrasonic data in 2D and soon in 3D at high frame rates, the ultrafast sequence can rely on much larger ensemble lengths in both time and space in order to discriminate tissue and probe motion from blood flow. Thus, the multidimensional SVD filter outperforms conventional temporal filters and leads to better discrimination because it takes into account large spatial ensemble lengths and the average statistics of the complete image is included. Finally, even in the most difficult situation where tissue motion is not completely stationary but rather low frequency and quite local, the SVD filtering works effectively to discriminate it from blood flow due fractal intrinsic properties of the vasculature. Indeed, the fractal nature of the vasculature implies that very low blood flows are present almost only in very small vessels much smaller than typical regions of tissues affected by the same range of motion. As their spatial statistics are different, the temporal variations of tissue and blood flow are nicely separated.

SVD filtering should have an important impact in the field of fUltrasound (functional ultrasound imaging of brain activity) since local hemodynamic changes linked to neurovascular coupling occur mainly in very small vessels where the blood flow speed is not measurable with conventional approaches. Moreover, the application of SVD filtering to ultrafast Doppler in the brain will be of particular interest for fUltrasound brain imaging of awake and freely moving animals where the optimal discrimination between tissue/probe motion artifacts and blood flow in small vessels becomes crucial.

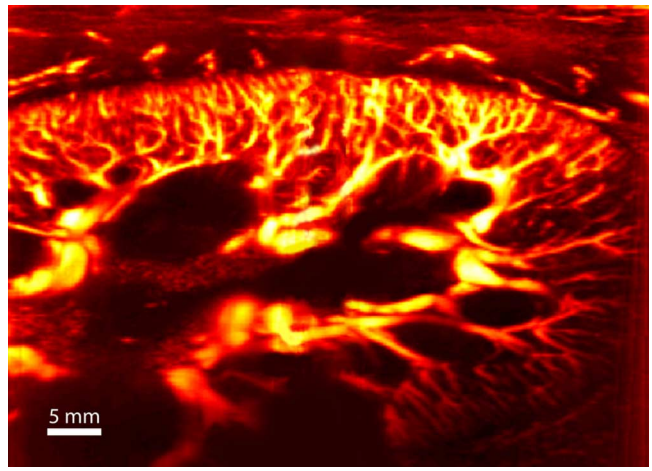

Fig. 14. Fusion (side to side concatenation with manual coregistration) of 2 Doppler images acquired in the same plane respectively on the left and right sides of the transplanted kidney of a human patient. The images are filtered via SVD filtering. The in vivo vascular network of the transplanted human kidney is delineated with a very high sensitivity without requiring the use of contrast agent.

The SVD clutter rejection also improves sensitivity and motion filtering in clinical applications such as kidney, liver, thyroid, heart imaging (data not shown). In this manuscript, results in neonate brain (Fig. 8 to Fig. 11), child liver and transplanted kidney (Fig. 13) were presented to illustrate the interest of this processing but many other unpresented data were acquired in thyroid and cardiac imaging and lead to the same conclusions. Neonate brain imaging is an interesting example of imaging application where it is difficult to ask patients to hold their breath. In such situations respiration motion combined to the ever-present pulsatility motion, are unavoidable. It is then difficult to filter out optimally slowly moving tissue from slow blood flow signal with a butterworth filter. In the liver example shown (Figs. 13(a) and 13(b)), tissue motion requires a 120Hz cut off frequency for the temporal filter and consequently vessels with blood speed below 1.5 cm.s^{-1} disappeared of the image, whereas SVD filtering is able to reject clutter without losing those small vessels. In the kidney example shown (Figs. 13(c) and 13(d)), tissue can be filtered out with a 90Hz cut off frequency for the temporal filter, and the blood flow speeds are consequent in most vessels (> 1.2 cm.s^{-1}), however SVD filtering still improves detection on venous structures in the central part of the image (long arrow) that present very low flow speeds ($\sim 0.8 \pm 0.2$ cm.s^{-1}) and completely disappear with temporal filtering. It is the same for deep small vessels whose signal is quite weak due to absorption (small arrow) and that can be quickly filtered out by a temporal filter. The sensitivity of Ultrafast Doppler combined with the discrimination capabilities of SVD filtering offers a level of detection never reached before with an ultrasound modality, even with the use of contrast agent (Fig. 14).

SVD clutter rejection is a powerful and versatile tool for Ultrafast Doppler imaging filtering, effective in many clinical applications. However this study presents some limitations, and a lot of areas for improvement have to be investigated. The first point is that no adaptive method for the choice of the threshold used for singular vector rejection has been proposed, but this is mainly due to the fact that the adjustment of this value is not as critical as for cut off frequency choice. It can be noticed that in all the examples presented in this paper a threshold of 80 rejected singular values would have given images with good quality, whereas temporal filter had to be precisely adjusted to reject clutter, with cut off frequencies ranging from 60 Hz to 250 Hz. However different strategies can be imagined for adaptive SVD clutter rejection: energy considerations on the level of the cumulative sum of the singular value can help, given an energy ratio in dB between blood signal and tissue signal depending on the acquisition parameters (ultrasound frequency, absorption coefficient . . .), to discriminate between the tissue subspace and the blood subspace of the singular vector space. A more sophisticated strategy is to calculate the central frequency of each individual temporal singular vector and to reject singular vector below a certain central frequency (a certain speed), strategy which do not overcome the problem of choosing a threshold because a certain speed has to be chosen, but which is adaptive to the amplitude of the motion present during the acquisition. Also, threshold can be dynamically chosen during the different phases of the cardiac cycle because the dimension of the tissue subspace increases for example during systole because of stronger tissue motion. These strategies will be presented with ongoing research in future work. Finally, the software beamforming capabilities provided by ultrasound scanners based on GPU boards [13] gives the physician the ability to adapt manually the singular value threshold to the desired image quality. This simplest strategy could turn out to be the most efficient compared to automatic approaches as the sonographers would rather manually optimize their image quality for different organs or patients.

Interestingly, robust and automatic approach for the choice of the filter threshold has been an extensive research topic in the applied mathematics community in the last decade. These approaches, i.e., the so-called Robust PCA [22], would permit to better choose the singular value thresholding. Our ultrasound problem fits to the context of robust PCA as the ultrasonic data acquired during ultrafast sequences can be seen as the superposition of a low-rank component (tissue motion) and a sparse component (blood motion).

First of all, the singular values of a random Gaussian matrix which corresponds to the noise component in (1) follows a Marchenko-Pastur distribution. This property can be taken benefit from to directly determine a rough statistical threshold by using Stein's Unbiased Risk Estimator (SURE method) as discussed by Candes *et al.* and Donoho *et al.* [21], [32]. In particular, Candes *et al.* applied the SURE method in order to determine an automatic threshold for the SVD decomposition in the context of dynamic MRI processing. In particular, they demonstrated the efficient use of the singular value thresholding (SVT) unbiased risk estimate for automated and optimized denoising of dynamic cardiac MRI series. The SURE method clearly demonstrated an improved assessment of myocardial perfusion. In this approach, the thresholding of singular values is not a hard-thresholding rule (*ie* replacing a subset of singular values by zeros), but rather introduce a soft-thresholding rule consisting in shrinking the singular values towards zero by a constant amount to determine during an iterative process. The outperformance of this more sophisticated approach will be evaluated in further works. Conversely to the other estimation approaches cited in Candes paper, we want to get rid of the main signal. Noise is present in addition to the blood signal in the low singular values subspace. However, as noted on Fig. 8(b), tissue signals (black curve) are 30 dB higher than blood flow signals (red curve) and blood flow signals are approximately 30 dB higher than the electronic noise level (tails of red curve). The accuracy and precision of local velocity estimation was studied both theoretically and experimentally in a previous paper using the same research platform [33].

Beyond the phantom study that provided quantitative Contrast to Noise Ratio data on the efficiency of SVD filtering compared to well-known other filtering algorithms, several points remain to clarify with quantitative data and controlled conditions, and will be addressed in future work. The range of tissue velocity explored in that phantom study has to be increased to cover high motion application, such as cardiac imaging, and the influence of the vessel size on the SVD filtering CNR has to be investigated and compared with other gold standard filters. Also, this study covered in plane tissue motion, but should also quantify the influence of out of plane motion.

The influence of the ensemble length has been underlined in this paper in terms of a comparison between really short ensembles (focused ultrasound) and very long ensembles (plane wave acquisitions). However the ensemble size used to build the Casorati matrix prior to SVD filtering has to be studied carefully, because it will be closely related to real-time capability of SVD filtering. In particular, temporal sliding windows or spatial-block processing will be investigated to find potential tradeoff between clutter rejection and computation time.

Computation is generally a bottleneck for real time imaging. With the current Matlab® implementation, and on an average quad core Xeon 2.66 GHz, the time to compute the SVD filtering is 0.5 s for a ($100 \times 128 \times 256$) Ultrafast acquisition, 1.7s for a ($100 \times 128 \times 512$) Ultrafast acquisition, 3.4 s for a ($200 \times 128 \times 512$) Ultrafast acquisition, and tend to be linear with the increase of the number of points in space and quadratic with the increase of the number of points in time (due to the choice of the covariance matrix presented in the method section). It is then indubitable that with the currently available processors, a reasonable choice for the processed temporal length of the Ultrafast Doppler acquisition and fastest C++ or GPU implementation, real time SVD filtering is reachable starting today.

Clinical data presented in this paper have been acquired with linear array and relatively high ultrasound frequency (6 MHz and 15 MHz). However this is not exclusive of other configuration and current work in our lab are conducted using Doppler SVD filtering with lower emission frequencies or phased array with diverging waves. Latest results on 3D ultrafast imaging rely on the use of SVD filtering with a 3 MHz probe and plane and diverging waves.

For some applications requiring very high performance levels for clutter filtering, the multidimensional SVD filter will be-

come mandatory. It is the case for human brain ultrasound functional imaging, because freehand imaging of neurovascular coupling rest upon detection of really slow blood flow in arterioles and venules. Tremendous sensitivity of Ultrafast Doppler combined to optimal filtering abilities of SVD clutter rejection is a milestone toward that end. In cardiac imaging, the detection of myocardium vascularization without any contrast agents in the fast moving cardiac muscle would also strongly benefit from the use of such SVD approaches. Osmanski *et al.* proposed for Ultrafast Doppler imaging a demodulation approach for the discrimination of myocardium blood and tissue motion in 2012 [34]. The SVD clutter filtering can outperform this approach for the visualization of coronary arteries without contrast agents. Such high sensitivity vascular imaging without contrast agents could also be interesting for tumor vascularization characterization as blood flow in the tumor micro vascularization is today impossible to detect due to limited cut-off frequency thresholds of classical clutter filters necessary to cancel tissue motion artifacts.

Finally, it has been shown in this article that the SVD filter performance is increasing with the ensemble length both in space and time, this is the reason why SVD filtering applied on 2D spatial data provided by ultrafast imaging outperforms SVD filtering applied to 1D spatial data provided by conventional focused emissions. For this reason, the extension of SVD clutter filtering to 4D ultrasonic data (3D space + 1D time) provided by ultrafast matrix arrays [35] should lead to even better results and an additional improvement of filtered data in 3D Ultrafast Doppler imaging.

REFERENCES

[1] S. Bjaerum, H. Torp, and K. Kristoffersen, "Clutter filter design for ultrasound color flow imaging," *IEEE Trans. Ultrason. Ferroelectr. Freq. Control*, vol. 49, no. 2, pp. 204–216, Jun. 2002.

[2] J. C. Willemetz, A. Nowicki, J. J. Meister, F. De Palma, and G. Pante, "Bias and variance in the estimate of the Doppler frequency induced by a wall motion filter," *Ultrason. Imag.*, vol. 11, no. 3, pp. 215–225, Jul. 1989.

[3] C. Tysoe and D. H. Evans, "Bias in mean frequency estimation of Doppler signals due to wall clutter filters," *Ultrasound Med. Biol.*, vol. 21, no. 5, pp. 671–677, 1995.

[4] Y. M. Yoo, R. Managuli, and Y. Kim, "Adaptive clutter filtering for ultrasound color flow imaging," *Ultrasound Med. Biol.*, vol. 29, no. 9, pp. 1311–1320, Sep. 2003.

[5] A. P. Kadi and T. Loupas, "On the performance of regression and step-initialized IIR clutter filters for color Doppler systems in diagnostic medical ultrasound," *IEEE Trans. Ultrason. Ferroelectr. Freq. Control*, vol. 42, no. 5, pp. 927–937, Sep. 1995.

[6] A. P. G. Hoeks, J. J. W. van de Vorst, A. Dabekaussen, P. J. Brands, and R. S. Reneman, "An efficient algorithm to remove low frequency Doppler signals in digital Doppler systems," *Ultrason. Imag.*, vol. 13, no. 2, pp. 135–144, Apr. 1991.

[7] L. Thomas and A. Hall, "An improved wall filter for flow imaging of low velocity flow," in *Proc. IEEE Ultrason. Symp.*, 1994, vol. 3, pp. 1701–1704.

[8] S. Bjaerum, H. Torp, and K. Kristoffersen, "Clutter filters adapted to tissue motion in ultrasound color flow imaging," *IEEE Trans. Ultrason. Ferroelectr. Freq. Control*, vol. 49, no. 6, pp. 693–704, Jun. 2002.

[9] L. A. F. Ledoux, P. J. Brands, and A. P. G. Hoeks, "Reduction of the clutter component in Doppler ultrasound signals based on singular value decomposition: A simulation study," *Ultrason. Imag.*, vol. 19, no. 1, pp. 1–18, Jan. 1997.

[10] A. C. H. Yu and L. Lovstakken, "Eigen-based clutter filter design for ultrasound color flow imaging: A review," *IEEE Trans. Ultrason. Ferroelectr. Freq. Control*, vol. 57, no. 5, pp. 1096–1111, May 2010.

[11] L. Lovstakken, S. Bjaerum, K. Kristoffersen, R. Haaverstad, and H. Torp, "Real-time adaptive clutter rejection filtering in color flow imaging using power method iterations," *IEEE Trans. Ultrason. Ferroelectr. Freq. Control*, vol. 53, no. 9, pp. 1597–1608, Sep. 2006.

[12] D. E. Kruse and K. W. Ferrara, "A new high resolution color flow system using an eigendecomposition-based adaptive filter for clutter rejection," *IEEE Trans. Ultrason. Ferroelectr. Freq. Control*, vol. 49, no. 10, pp. 1384–1399, Oct. 2002.

[13] M. Tanter and M. Fink, "Ultrafast imaging in biomedical ultrasound," *IEEE Trans. Ultrason. Ferroelectr. Freq. Control*, vol. 61, no. 1, pp. 102–119, Jan. 2014.

[14] J. Bercoff, M. Tanter, and M. Fink, "Supersonic shear imaging: A new technique for soft tissue elasticity mapping," *IEEE Trans. Ultrason. Ferroelectr. Freq. Control*, vol. 51, no. 4, pp. 396–409, Apr. 2004.

[15] M. Tanter, J. Bercoff, L. Sandrin, and M. Fink, "Ultrafast compound imaging for 2-D motion vector estimation: Application to transient elastography," *IEEE Trans. Ultrason. Ferroelectr. Freq. Control*, vol. 49, no. 10, pp. 1363–1374, Oct. 2002.

[16] G. Montaldo, M. Tanter, J. Bercoff, N. Benech, and M. Fink, "Coherent plane-wave compounding for very high frame rate ultrasonography and transient elastography," *IEEE Trans. Ultrason. Ferroelectr. Freq. Control*, vol. 56, no. 3, pp. 489–506, Mar. 2009.

[17] J. Bercoff *et al.*, "Ultrafast compound Doppler imaging: Providing full blood flow characterization," *IEEE Trans. Ultrason. Ferroelectr. Freq. Control*, vol. 58, no. 1, pp. 134–147, Jan. 2011.

[18] E. Mace *et al.*, "Functional ultrasound imaging of the brain: Theory and basic principles," *IEEE Trans. Ultrason. Ferroelectr. Freq. Control*, vol. 60, no. 3, pp. 492–506, Mar. 2013.

[19] C. R. Cooley and B. S. Robinson, "Synthetic focus imaging using partial datasets," in *Proc. IEEE Ultrasonics Symp.*, 1994, vol. 3, pp. 1539–1542.

[20] E. Macé *et al.*, "Functional ultrasound imaging of the brain," *Nat. Methods*, vol. 8, no. 8, pp. 662–664, Jul. 2011.

[21] E. J. Candes, C. A. Sing-Long, and J. D. Trzasko, "Unbiased risk estimates for singular value thresholding and spectral estimators," *IEEE Trans. Signal Process.*, vol. 61, no. 19, pp. 4643–4657, Oct. 2013.

[22] E. J. Candès, X. Li, Y. Ma, and J. Wright, "Robust principal component analysis?," *J. ACM JACM*, vol. 58, no. 3, p. 11, 2005.

[23] R. Otazo, E. Candès, and D. K. Sodickson, "Low-rank plus sparse matrix decomposition for accelerated dynamic MRI with separation of background and dynamic components," *Magn. Reson. Med.*, vol. 73, no. 3, pp. 1125–1136, Mar. 2015.

[24] H. Gao, H. Yu, S. Osher, and G. Wang, "Multi-energy CT based on a prior rank, intensity and sparsity model (PRISM)," *Inverse Probl.*, vol. 27, no. 11, p. 115012, Nov. 2011.

[25] Y. H. Sajan Goud Lingala, "Accelerated dynamic MRI exploiting sparsity and low-rank structure: k-t SLR," *IEEE Trans. Med. Imag.*, vol. 30, no. 5, pp. 1042–54, 2011.

[26] Z.-P. Liang, "Spatiotemporal imaging with partially separable functions," in *Proc. NFSI-ICFBI*, 2007, pp. 181–182.

[27] C. Eckart and G. Young, "The approximation of one matrix by another of lower rank," *Psychometrika*, vol. 1, no. 3, pp. 211–218, Sep. 1936.

[28] B. F. Osmanski *et al.*, "Functional ultrasound imaging reveals different odor-evoked patterns of vascular activity in the main olfactory bulb and the anterior piriform cortex," *NeuroImage*, vol. 95, pp. 176–184, Jul. 2014.

[29] B. F. Osmanski, S. Pezet, A. Ricobaraza, Z. Lenkei, and M. Tanter, "Functional ultrasound imaging of intrinsic connectivity in the living rat brain," *Nature Commun.*, Oct. 2014.

[30] C. Demené *et al.*, "Ultrafast Doppler reveals the mapping of cerebral vascular resistivity in neonates," *J. Cereb. Blood Flow Metab.*, Mar. 2014.

[31] K. P. Ivanov, M. K. Kalinina, and Y. I. Levkovich, "Blood flow velocity in capillaries of brain and muscles and its physiological significance," *Microvasc. Res.*, vol. 22, no. 2, pp. 143–155, Sep. 1981.

[32] D. Donoho and M. Gavish, "Minimax risk of matrix denoising by singular value thresholding," *Ann. Stat.*, vol. 42, no. 6, pp. 2413–2440, Dec. 2014.

[33] T. Deffieux, J.-L. Gennisson, B. Larrat, M. Fink, and M. Tanter, "The variance of quantitative estimates in shear wave imaging: Theory and experiments," *IEEE Trans. Ultrason. Ferroelectr. Freq. Control*, vol. 59, no. 11, Nov. 2012.

[34] B.-F. Osmanski *et al.*, "Ultrafast Doppler imaging of blood flow dynamics in the myocardium," *IEEE Trans. Med. Imag.*, vol. 31, no. 8, pp. 1661–1668, Aug. 2012.

[35] J. Provost *et al.*, "3D ultrafast ultrasound imaging in vivo," *Phys. Med. Biol.*, vol. 59, no. 19, p. L1, Oct. 2014.